Control and support of 4-meter class secondary and tertiary mirrors for the Thirty Meter Telescope

Dan Blanco[†a], Myung Cho[a], Larry Daggert[a], Phil Daly[a], Joe DeVries[a], Jonathan Elias[a], Bruce Fitz-Patrick[a], Ed Hileman[a], Mark Hunten[a], Ming Liang[a], Mark Nickerson[a], Earl Pearson[a], Dave Rosin[a], Mark Sirota[b], Larry Stepp[b]

[a]NOAO, 950 N. Cherry Avenue, Tucson, AZ, USA 87544
[b]TMT Project, 2632 East Washington Blvd, Pasadena, CA, USA 91107

ABSTRACT

The Thirty Meter Telescope (TMT) project is a partnership between ACURA, AURA, Caltech, and the University of California. The design calls for a 3.6 m diameter secondary mirror and an elliptical tertiary mirror measuring more than 4 m along its major axis. Each mirror will weigh more than two metric tons and must be articulated to compensate for deformation of the telescope structure. The support and control of these "smaller optics" pose significant challenges for the designers. We present conceptual designs for active and passive figure control and articulation of these optics.

Keywords: Mirror support, articulation, figure control, hexapod, extremely large telescopes

1. INTRODUCTION

The next generation of extremely large telescopes will have apertures roughly an order of magnitude larger than those of existing telescopes. These extremely large apertures imply very large secondary and tertiary mirrors. In the case of the Thirty Meter Telescope (TMT), both the secondary and tertiary mirrors are larger than 3 m in diameter. Support, positioning, and figure control of these optics are comparable to those for the primary mirror of a moderate-sized telescope.

The requirements for the tertiary are particularly complex, because TMT plans to mount instruments at a range of locations on the Nasmyth platforms. This allows efficient access to multiple instruments, but requires the tertiary to track both in elevation and azimuth as the telescope elevation changes. This implies a two-dimensional variation in the gravity vector, so the support requirements for this mirror are more like those for the primary of an equatorial telescope than for an alt-azimuth telescope.

At present, TMT is pursuing parallel development of two secondary mirror options - a conventional secondary (CM2) and an adaptive secondary[1]. This approach is primarily a risk-reduction strategy, since production of a conventional secondary ensures that telescope first light won't be delayed. Although the adaptive secondary is a demanding technical task, the requirements that it imposes on the remainder of the secondary mirror system are, if anything, less than for the conventional secondary. For this reason the discussions in this paper are focused on the CM2 implementation, which we refer to as simply M2.

When operating in the seeing-limited mode, the secondary mirror (M2) and the tertiary mirror (M3) must maintain their optical surfaces without independent wavefront sensor feedback. The segmented primary mirror (M1) with its large number of actively controlled degrees of freedom will be used to correct aberrations on the M2 and M3. The adaptive optics systems are also capable of providing correction at higher spatial frequencies and higher bandwidth. The M2 is close to the telescope pupil, but the M3 is not. As a consequence, the footprint of the beam on the M3 is quite different for different points over the full TMT field of view of 20 arcminutes. The intrinsic performance of M3 must be quite

[†] dblanco@noao.edu; phone 1 520 318-8246; fax 1 520 318-8424

good, since the ability of the primary mirror to correct off-axis performance is limited. The adaptive optics systems will also have difficulty in correcting for M3, for similar reasons.

The required performance can be achieved only if the mirrors' figures are accurately controlled. This control will be achieved by look-up tables to control the mirror supports. These tables will be derived from a combination of modeling, direct calibration of mirror performance (including periodic recalibration), and a planned global metrology system (GMS) which can be used at intervals during the night.

2. REQUIREMENTS OVERVIEW

The TMT image quality error budget allocates contributions to telescope subsystems based on residual errors after compensation. There are budgets for both the seeing-limited case and for use with adaptive optics (AO) systems; the M2 and M3 error budgets are driven primarily by the seeing limited case. The top-level error allowances shown in Figure 1 are the allowable residual errors after the following compensators:

- A flexure look-up table (LUT) to compensate for gravity deformation
- A pointing LUT
- Periodic recollimation using the GMS to compensate for thermal drift and creep
- M2 & M3 figure correction LUT's
- Instrument wavefront sensor feed back used to correct focus and coma
- Guider correction from instrument guide cameras
- M1 figure control based on instrument wavefront sensor

Rigid body displacements will be mapped with a GMS – a set of three laser trackers that use either "time of flight" or heterodyne interferometry to measure absolute distances to a fraction of a millimeter. A flexure LUT based on GMS is the first of a series of compensators, each correcting the image to within the capture range of the next.

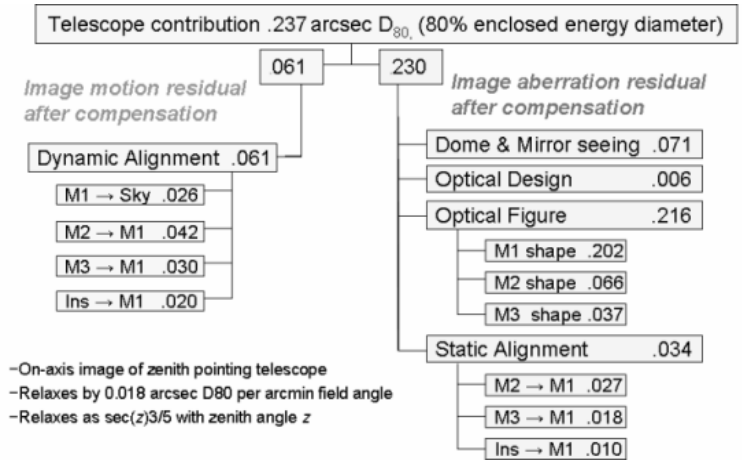

Figure 1. Top level seeing-limited error budget in terms of 80% image diameter. These are residual errors after several compensators that operate with both real time feed-back and from look-up table corrections.

We adopted the metric that shape error contributions should not exceed an equivalent atmospheric aberration. This assures that the residual seeing-limited error can be further corrected by AO. In terms of wavefront error, the allocations for M2 and M3 are 205 nm and 127 nm rms respectively. Wavefront error was the basis for a working error budget with the proviso that the accumulated errors should conform to a tilt-corrected structure function. In practice we expect to correct figure errors on M2 and M3 by measuring the on-axis wavefront and making aO corrections to the M1 figure. The resulting correction will have most effect for the on-axis image point, but will degrade with off-axis distance according to the initial aberration. For low order aberrations the correction is effective over the full 20 arcminute field provided that the small residual field distortion is acceptable.

Both M2 and M3 will be articulated; M2 will be mounted on a hexapod positioner to compensate for structural and thermal deformations, and to make small changes to accommodate the requirements of the various instruments. GMS will be used for initial collimation; this will obtain collimation sufficient to produce images that are better than 1 arcsec θ_{80}, within the capture range of wavefront sensors on board the science instruments. Focus and coma will be corrected by adjusting the M2 position, while higher order aberrations will be corrected by adjusting M1. To achieve the image blur residual allowance, the M2 position must be held to better than 3.1 microns in piston, 22 microns in centration, and 1.4 arcseconds in tilt (about 25 microns at the edge of M2). In operation M2 will be dynamically repositioned; to achieve the image motion allowance the tracking jitter must be within 0.54 microns and 0.054 arcseconds at any frequencies than are cannot be corrected by guider control of the telescope mount.

The M3 positioner superficially resembles a 4-m class alt-azimuth telescope mount, albeit one that is mounted on a platform that tilts up to 65º from vertical. To avoid confusion with the main telescope axes, the M3 coordinates are named rotation (about the optical axis) and tilt (about the M3 elevation axis). At zenith pointing the rotation axis is used to switch the beam between instruments deployed along the two Nasmyth platforms. Both tilt and rotation axes must move as the telescope tracks off-zenith to continuously steer the beam onto the instrument. Even when the beam is directed along the elevation axis, correction for structural deformations will require frequent repointing. The requirements on M3 positioning are 4.5 arcsec repeatability and 0.097 arcseconds jitter in both axes at frequencies that cannot be corrected by mount guider control. Though these requirements are less stringent than for M2, the M3 positioner must achieve this over a larger range of motion and speed.

3. M2 SUPPORT

Face-sheet configurations in low expansion glass or glass ceramic were selected for both mirrors, a choice dictated partly by economy, but largely to limit aberration residuals to low spatial frequencies. We have tentatively selected a 100 mm thickness as a reasonable compromise between manufacturability and low thermal inertia. M2 has a mechanical diameter of 3.65 m and a sagitta of approximately 266mm. Its center of gravity is located in free space 83 mm in front of the mirror vertex.

Goals for the M2 support system include:

- Provide active control with high stability to maintain accurate figure control from LUT corrections
- Low power dissipation (minimize heat released into the beam)
- High reliability with low maintenance
- Low mass
- Optionally, provide rapid tip tilt of M2

The prospect of rapid tip tilt on a four meter class optic is clearly non-trivial, but initial studies indicate that it may be feasible for small amplitudes (~1 arcsecond on the sky) and at modest frequencies near the telescope's first resonance (~5 Hz). During the concept design phase we have concentrated on development of a quasi-static support system, but the design allows a path for development towards rapid tip tilt.

The choice of supports was driven by the seeing limited mode; the requirement to operate without direct feedback from a wavefront sensor emphasizes the need for long-term stability of the support system. Of the various supports used in modern telescopes, hydraulic systems have consistently shown good stability. While hydraulic systems have demonstrated good performance, virtually all have leaked. The two most common sources of leaks have been connectors and rolling element style piston actuators. We intend to mitigate leaks by using aircraft grade connectors and hermetically sealed steel bellows actuators. As a final precaution, the system will use a relatively benign water-alcohol working fluid.

The M2 will be supported axially at sixty locations arranged in four concentric rings of 6, 12, 18, and 24 supports (Figure 2). This hexapolar arrangement provides a near-optimal support pattern; the ring radii were adjusted slightly to minimize figure error in axial loading. Sixteen lateral, and six cross-lateral supports are provided at the third ring.

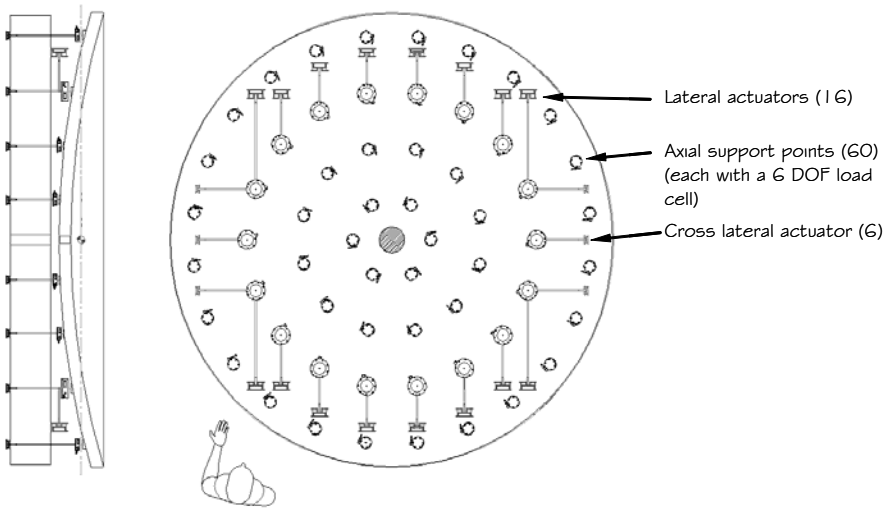

Figure 2. M2 support actuator layout. 60 axial supports are laid out in four concentric rings. All lateral loads are carried by supports on the third ring, co-located with axial supports using the same locations.

Each actuator couples to the mirror through three components; a push/pull rod, a universal flexure and a six-axis load cell. The push/pull rods provide decoupling between the lateral and axial supports to accommodate assembly errors, differential thermal expansion and the like; the universal flexure reduces parasitic moments from being transmitted from the supports into the mirror substrate and defines the location of the support force. The third component is a six-axis load cell. Experience with existing support systems indicates that figure errors often arise due to parasitic forces and moments that are not measured or controlled; we intend to preclude this by measuring *all* forces and moments that are transmitted into the substrate, to within the 1/8 N resolution of the load cells.

The axial actuators are divided into three 120 degree sectors kinematically defining three degrees of rigid body freedom; the lateral supports are divided into two zones and the cross lateral actuators comprise one zone defining the remaining degree of freedom. The three axial zones are further divided into eight sub zones on a common hydraulic manifold (Figure 3).

Figure control actuators apply differential pressure between zones enabling active warping of the mirror. Three sector valves are located at the interconnections of the 120 sectors. With sector valves closed, the system is kinematically constrained. When open the figure control actuators can be used to meter fluid between sectors tilting the mirror concurrent with warping action.

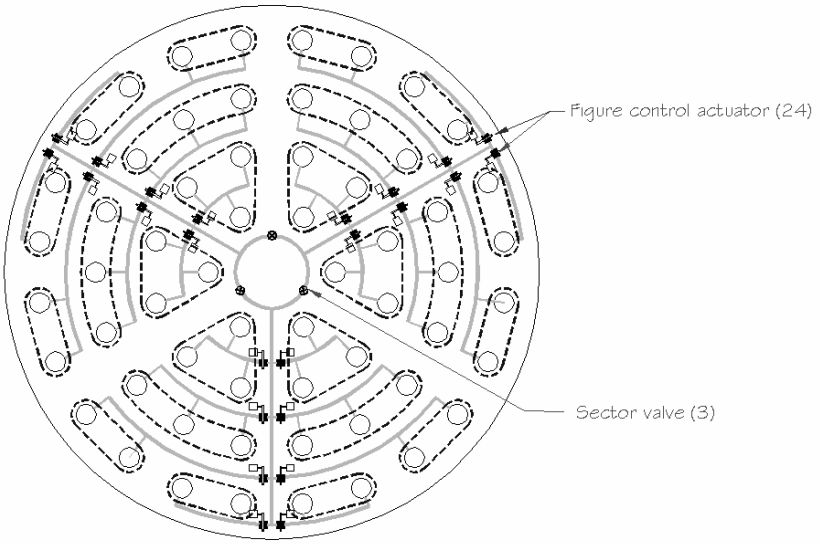

Figure 3. Partitioning of hydraulic zones for the axial supports. Figure control actuators apply differential pressure between a common manifold and a particular zone of two or three actuators. This may be used to affect warping forces on the mirror. When the sector valves are closed the mirror is kinematically defined. With the valves opened, fluid can be metered between sectors between sectors to tilt the optic.

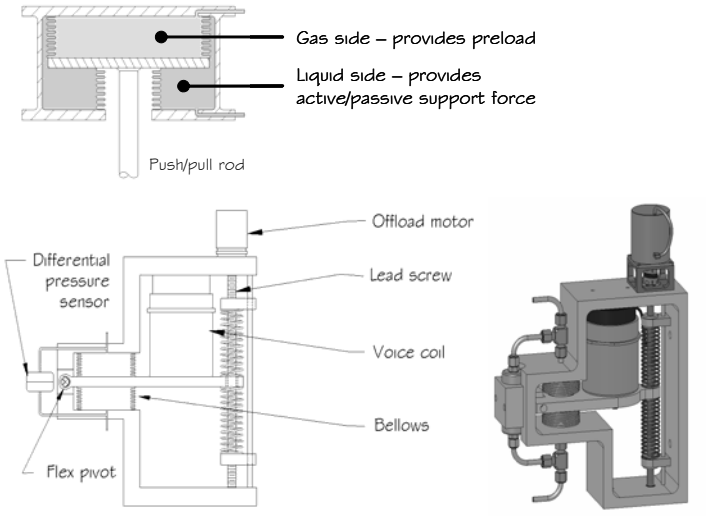

Figure 4. Bellows actuator (above) consists of two chambers, a liquid side with a gas side for preload and a liquid side. The liquid pressure is controlled by 24 figure control actuators shown below as a solid model (right), and schematic (left).

Each axial actuator consists of two chambers; one is fluid-filled and connected with the hydraulic circuit. The other chamber can be pressurized to provide an offset preload so that both push and pull forces can be applied (Figure 4). The figure control actuators consist of two steel bellows arranged on either side of a hinged paddle. Two force actuators can apply differential pressure between the bellows; a voice coil actuator can apply over 400 N peak force while a stepper motor, lead screw and linear spring arrangement can apply up to 200 N of constant force. The design allows pressure variations to communicate between the two bellows so that the hydraulic circuits function as a passive hydraulic whiffle tree when the actuators are not actively controlled. A differential pressure transducer provides feedback to a local controller to maintain a commanded differential pressure.

The mirror cell, shown cut away in Figure 5, serves as the 'hard point' to which the axial and lateral support actuators and the M2 positioning hexapods are mounted. The cell is designed to distribute loads from the actuators to three points where the hexapod assembly attaches in a stiff manner. It is desirable to minimize the cell weight to help limit top end deflection of the telescope and keep the structure economical. From several considered configurations, a steel weldment utilizing two parallel face sheets with a honeycomb core has been selected. Parallel face plates allow simplified fabrication and machining of critical interface surfaces where actuators and hexapods attach. Lateral actuators attach to separate brackets, which in turn bolt to machined surfaces on the lower cell face.

4. M2 OPTICAL PERFORMANCE

The mirror was modeled using solid finite elements and multiple point constraints (MPC). Optical performance was evaluated for support print-through, support error sensitivity, dynamic wind response, and the ability of the active support system to duplicate low order Zernike modes. In the optical surface calculations the region within the 200 mm central obscuration was ignored. Gravity induced mirror deformation was evaluated at zenith and horizon pointing. This is outside the maximum operating range of 65 degrees maximum zenith distance.

Axial supports were optimized at the zenith position to obtain minimum RMS surface deformation. The optimization predicts a surface RMS of 20 nm (see Figure 6) with axial forces in two groups; 350 N on the inner most ring of six supports and 430 N on the remaining 54 supports. Lateral support optimization done at horizon pointing predicted a surface RMS of 82 nm after applying figure correction with the axial supports applying a maximum 182 N force. The lateral support system was a compromise between design simplicity and performance; better performance can be achieved with more complex designs, but the relatively simple sixteen-point design we selected is expected to meet our specification.

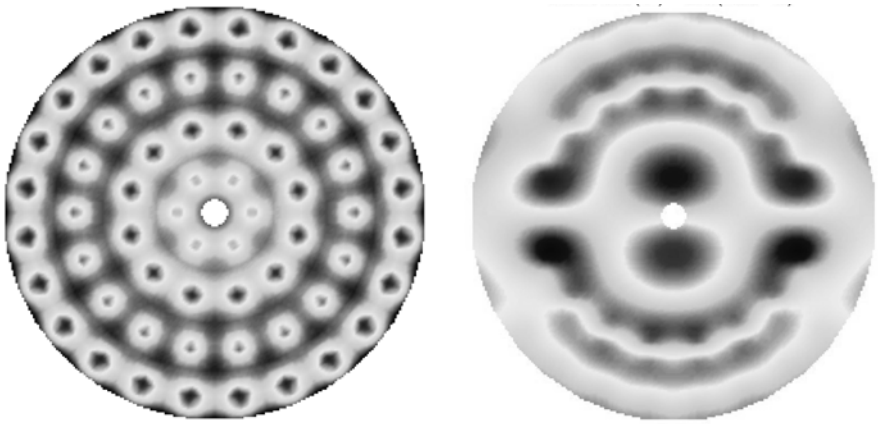

Figure 6. Surface print-through at zenith pointing (right) is 20 nm RMS. At due horizon pointing (left) the surface print-through is 82 nm RMS after applying figure correction with the axial active supports.

A single axial force error of 1 N produces a net change in the optical surface of 5.7 nm surface RMS in an astigmatic shape. A sample of ten FE models with +/- 0.25 N axial force errors in random three-sigma Gaussian distribution produced an average 4.3 nm RMS surfaces with predominantly astigmatic shapes. A complete failure of a single support changes the surface from 20 nm to 92.8 nm RMS after re-optimizing the remaining active support forces. A single lateral support misplaced by 1 mm along the optical axis, equivalent to an offset moment of 1.6 N-m, changes the surface from 82 nm to 93 nm RMS. A complete failure of a lateral support changes the surface from 82 nm to 99 nm RMS after re-optimizing the active forces.

CFD models of the TMT telescope and enclosure[2] yielded estimated wind loading force of 16.7 N (steady) and RMS force variations of 26.1 N. We assumed a random distribution of wind induced forces. Based on thirty sample cases, the average optical surface deformation is 8.0 nm RMS. The deformed optical surfaces were strongly dominated by astigmatic shapes.

The performance of the 24-zone active support system is summarized in Table 1. The forces in each of the 24 zones were optimized to warp the mirror into each of the first 24 Zernike modes in turn. The twelve modes with the largest gain, defined as the ratio of the RMS input amplitude (1000 nm in each case), to the RMS residual error. The maximum forces required to obtain 100 nm RMS surface amplitudes are recorded along with the residual surface error and the "gain" (the ratio of the RMS input to the residual error).

It is desirable to apply the active support system to correct errors from potential external or internal loads. To demonstrate this, a thermal gradient case was considered. This assumed a linear gradient of 1C along the thickness, with the top surface warmer than the back surface. For this particular case, a surface P-V of 850 nm and RMS of 247 nm were calculated (in a strong focus shape) before active correction. After applying active support correction the optical surface RMS was reduced to 8 nm with a maximum correction force of 18 N.

Table 1. Performance of the 24-zone active support system; maximum force, residual error, and gain for twelve Zernike mode shapes closest to the natural bending modes of the secondary mirror ranked according to gain.

Zernike mode		*Fmax (N)*	*RMS (nm)*	*Gain*
6	astig	2.0	0.8	121.5
5	astig	2.2	0.8	118.9
10	3-foil	6.2	2.5	40.4
9	sphr	63.0	4.1	24.7
11	3-foil	3.9	6.2	16.1
7	coma	34.2	10.1	9.9
8	coma	28.7	10.2	9.8
18	4-foil	15.8	10.6	9.4
17	4-foil	17.9	10.7	9.4
16	5th sphr	222.2	13.0	7.7
13	5th coma	68.0	26.9	3.7
12	5th coma	78.5	27.0	3.7

5. M3 SUPPORT

The M3 presents a particular challenge both for its unprecedented size and because of the two-dimensional variation in the gravity vector. Several considerations drove us to an unusual design approach:

- Keep edge of optic clear of hardware (avoid obscuration of M1)
- Avoid coring into back of optic (fabrication risk, source of high frequency figure error)
- Avoid counterweights (vibration, weight, and handling issues)
- Maximize passive performance (less active correction required)
- Lateral loading occurs in two orthogonal directions (multiplies complexity)

The M3 is similar in size and aspect ratio to M2, so a sixty-point support pattern was selected with supports arranged in four elliptical rings of 6, 12, 18 and 24 supports.

Several types of supports were considered leading to the selection of a passive, static, hydraulic support system. The support actuator concept is shown in Figure 7. This is a tri-axial design combining three individual actuators inclined to one another such that their lines of action intersect at the midplane of the 100 mm thick face sheet. All support loads pass through a multi-axis load cell before reaching the mirror back face. The three lines of action are orthogonal to one another to decouple their action. This configuration supplies both axial and both directions of lateral support.

Hydraulic connection of the actuator bellows is illustrated in Figure 8. Bellows sharing a common direction are divided into two opposing zones, the actuators of each zone being interconnected hydraulically. This scheme is extended to all actuator directions, ***i***, ***j***, and ***k***. The net result is kinematic constraint in all six degrees of freedom.

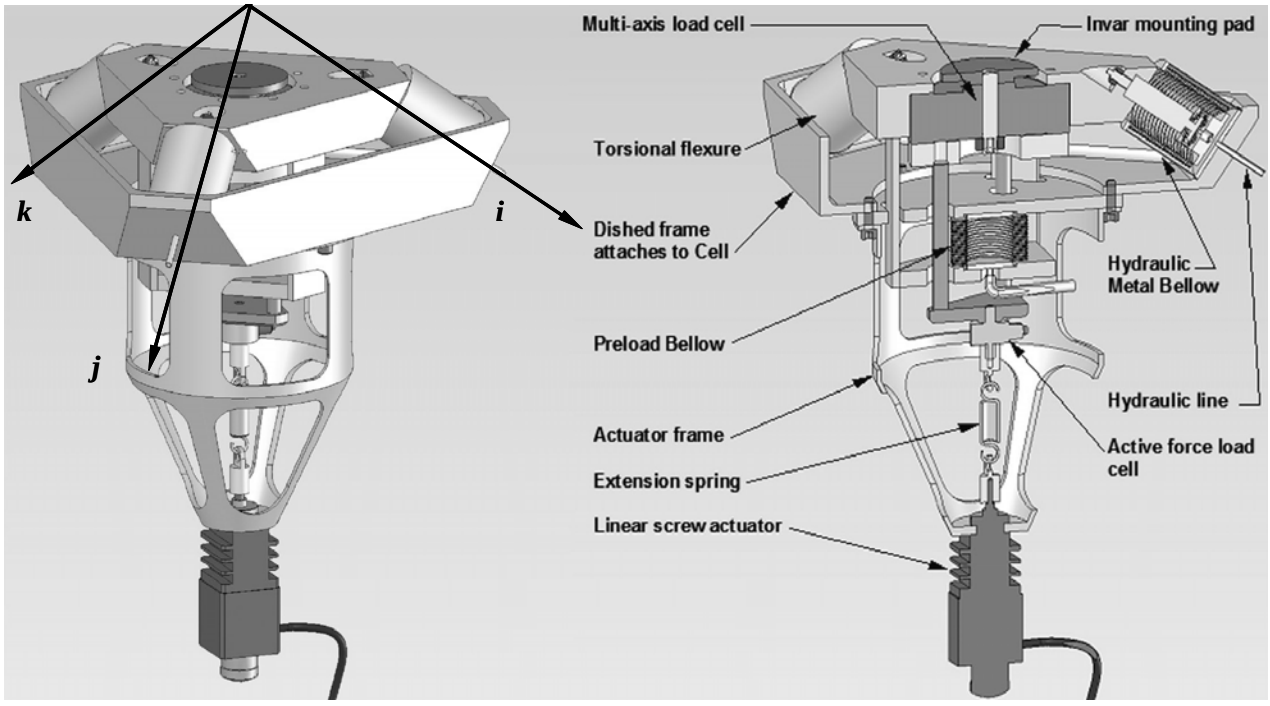

Figure 7. M3 support actuator concept. Orthogonal tripod arrangement of individual bellows actuators provides both axial and lateral support. Lines of action through bellows intersect at mirror mid plane. All support forces pass through a multi-axis load cell prior to reaching back of mirror where forces and moments in all six DOF are measured.

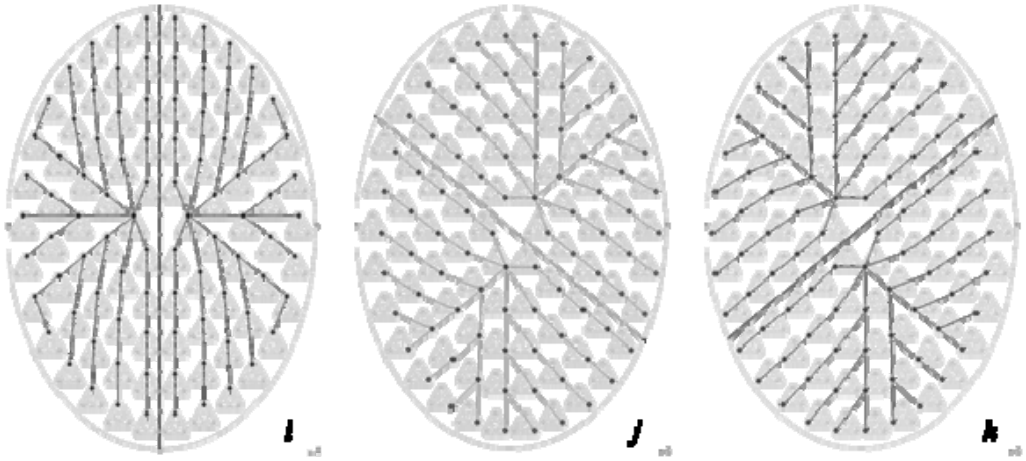

Figure 8. Hydraulic connection schematic for the support actuators. Two circuits, divided into opposing zones, interconnect bellows having a common direction. This arrangement is repeated for all **i**, **j**, and **k** actuator directions. Kinematic constraint in all six degrees of freedom is achieved.

Figure correction via active axial force control is incorporated into the lower portion of the actuators by addition of a linear drive motor acting through a tension spring (refer to Figure 6). Varying the spring extension between actuators causes differential axial forces at the support points, which may be used to warp the optic correcting for gravity and thermally induced low frequency errors. A separate load cell dedicated to measuring only the active component is utilized for high resolution feedback to the control system. It will be necessary to preload the hydraulic circuits in order to maintain positive pressure at all gravity orientations. This is accomplished by use of a separate, axially acting preload bellow in each actuator. A common regulated pneumatic pressure is provided to all preload bellows. Fluid may be used as an alternative. With appropriate sizing, use of fluid in the preload circuit can compensate differential head pressure arising in the hydraulic bellow circuits. A layout of the M3 mirror supports, cell and figure control actuators is shown in Figure 9.

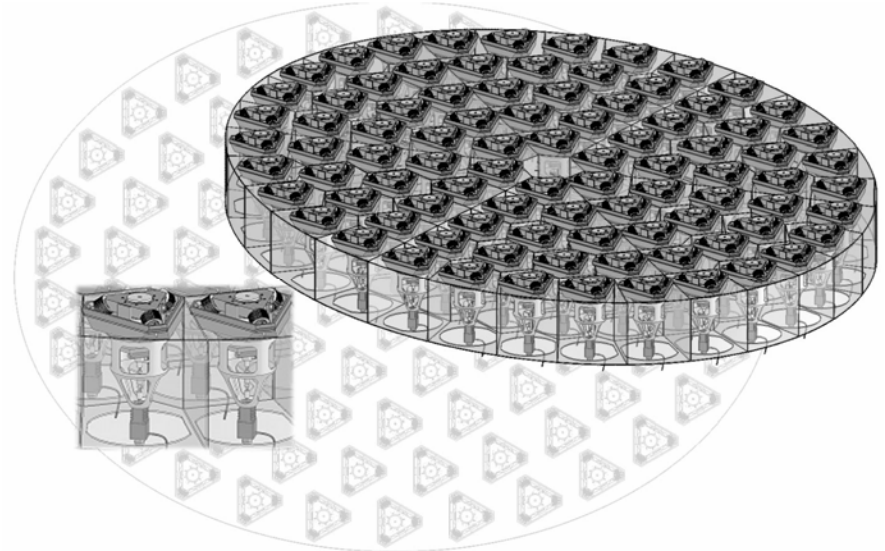

Figure 9. All sixty actuators installed within the M3 cell. Actuator design allows disassembly through back face of cell. After first removing active portion of actuator (lower section), interface between actuator and bonded pad can be separated, allowing removal of the passive section (upper portion) as a unit.

6. M3 OPTICAL PERFORMANCE

The mirror support system was modeled using solid finite elements and multiple point constraints that modeled the kinematic definition of the support system. In operation the gravity loading varies in all three orthogonal directions; performance was assessed at the three extreme conditions for gravity acting in X, Y or Z. Each of these is outside the range of normal operations. Optical performance was evaluated for support print-through, support error sensitivity, dynamic wind response, and the ability of the active support system to duplicate low order Zernike modes. Gravity induced mirror deformation was evaluated at each orientation. Zernike coefficients were determined over an aperture normalized to the beam footprint. The M3 axial support system was optimized to minimize the RMS surface deformation. The optimization predicted a surface RMS of 18.2 nm with nominal passive axial forces in two groups (nominally 310 N on the inner most ring and 410 N on the rest). The tri-axial support mechanisms were modeled with attachments at the back of the mirror blank. This yielded minimal lateral support print-though effects. The optical surface RMS errors are nominally 1 nm for both lateral cases (X-gravity and Y-gravity). The residual error maps for the optimized supports in gravity loading three orthogonal directions are shown in Figure 10.

Figure 10. Support print-through in Z gravity loading (right, 20 nm), and lateral loading in X and Y (right, both 1 nm RMS).

Sensitivity and tolerance analyses on M3 are similar to the M2 analyses previously discussed. A single axial support on the fourth ring was assumed to fail, resulting in zero axial force. In this case, the surface RMS changed to 78.7 nm from 18.2 nm after re-optimizing the remaining active supports. For a case in which a single axial support has a force error of 1 N, the net change in the optical surface error is less than 1 nm surface RMS after active optics corrections. The line of action in the tripod mechanism must be carefully maintained. For the case in which a single lateral support is misplaced by 1mm along the optical axis (Z axis), equivalent to applying an offset moment of 0.4 N-m at that support, the net change of 4.1 nm surface RMS for Y-gravity and 3.7 nm for the X-gravity loading. For the case that the entire lateral supports are mislocated by 1 mm along the Z-axis, the net change of 60.3 nm surface RMS for the X-gravity and 56.8 nm for the Y-gravity. Uncertainty in the active force was modeled by applying axial force errors of +/- 0.25 N in a three-sigma random Gaussian distribution. Ten random distributions models were used to predict the optical deformations as a first order approximation. The optical surface RMS is estimated at 4.6 nm on average. The deformed optical surfaces show dominant astigmatic shapes.

Wind loadings at M3 were assumed to be attenuated to 65% of the outside wind velocity. This is estimated to produce wind loads of 26.7 N (steady) and RMS force variations of 2.8 N, and a force of 1.9 N linearly distributed along the local Y-axis (high in –Y). Thirty models with randomly distributed wind loads yielded an average 18 nm RMS surface error. The deformed optical surfaces were strongly dominated by astigmatic shapes.

In order to evaluate the M3 active optics performance, the first ten natural mirror bending modes were considered as shown in Figure 11. Each mirror bending mode was scaled to a 1000 nm amplitude. The active optics performance for each mode is summarized in Table 2. We also applied active optics corrections for a few low order Zernike modes. In

general, these require higher corrective forces and have larger residual errors than the natural bending modes, a natural consequence of the non-circular M3.

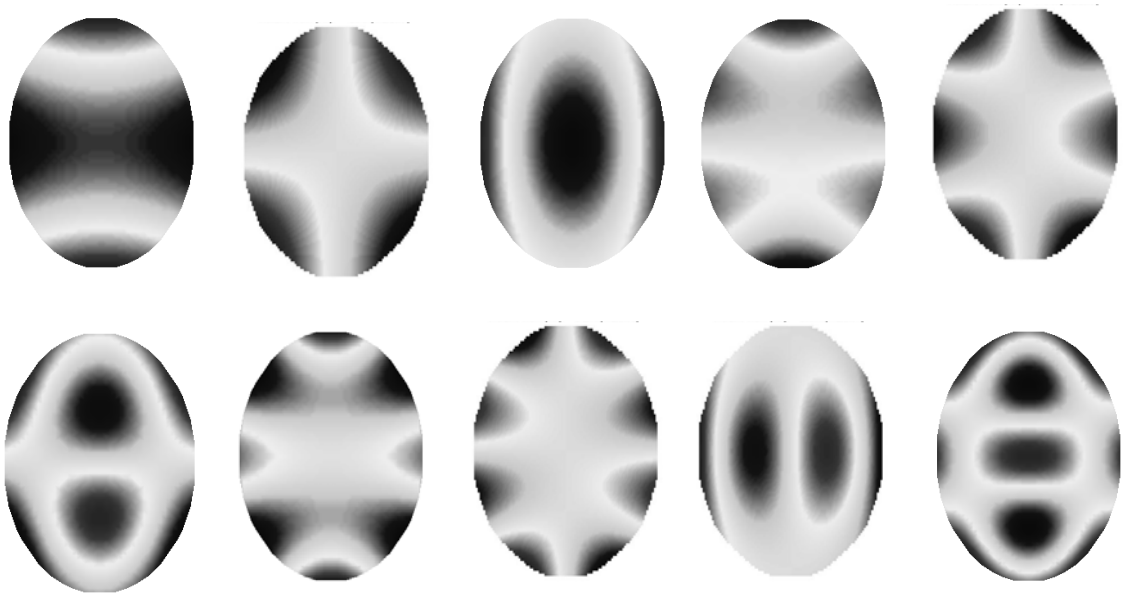

Figure 11. The first ten natural bending mode shapes for the tertiary mirror.

As discussed in the sensitivity section, the lateral support is sensitive to offsets of the line of action of the tri-axial support mechanisms, particularly along the Z axis. It highly desirable to apply active corrections to correct errors associated with the lateral support systems. With this active optics correction, the optical performance will be improved significantly for any lateral support misposition. In the case of an offset of 1 mm, the optical surface errors can be corrected almost entirely (residual RMS of 0.3 nm) from RMS of 60.3 nm with a maximum active force of 1.8 N. We also modeled the active optics performance with a thermal gradient case. This case assumed a linear gradient of 1 C along the mirror thickness, with the top surface 1C warmer than the back surface. For this particular case, a surface RMS of 255 nm was calculated in a strong focus shape prior to active optics corrections. After applying active optics correction the optical surface RMS was reduced to 5.5 nm with a maximum active correction force of 17 N.

Table 2. Maximum force, residual RMS surface error, and gain for the first ten natural bending modes shown in figure 12. Each mode was scaled to 1000nm RMS surface error.

Mode #	P-V (nm)	Fmax (N)	RMS (nm)	Gain
1	3982.2	6.7	0.2	4077
2	4551.7	8.7	0.3	3675
3	4115.7	28.9	1.1	927
4	5529.5	40.2	1.7	587
5	4963.1	43.8	1.6	644
6	4360.0	81.0	5.9	170
7	5187.2	124.4	6.0	168
8	5616.1	136.4	5.5	183
9	4882.6	162.5	7.2	139
10	4187.8	318.8	22.5	44

7. M2 POSITIONER

The M2 positioner will provide quasi-static articulation for the M2 payload in five DOF. Several alternative positioner systems were studied early in the design process leading to the selection of a hexapod as most likely to meet our design requirements. The required size, resolution and repeatability make this particularly challenging. CSA Engineering

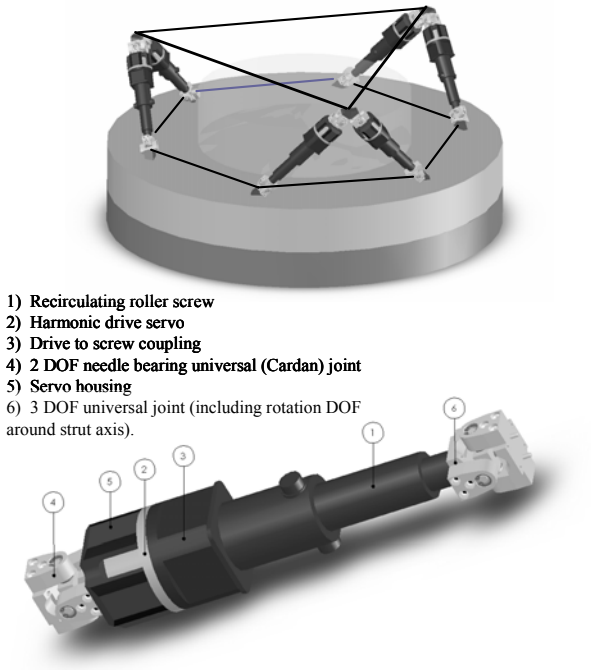

Figure 12. Hexapod positioner layout and strut detail.

(www.casengineering.com) was contracted to perform concept design study and feasibility assessment for a hexapod that would meet the design requirements in Table 3.

The working envelope for the hexapod is constrained to an overall height of 1.0 m and a maximum diameter of 3.5 m. The cell attachment interface was chosen to be at a 3.0 m diameter with six equally spaced attachment points. These constraints allowed some room for optimizing. The angle between the strut joint nodes and height between the top and bottom strut joint nodes were chosen as variables for the geometry optimization (Figure 12) to obtain an optimal compromise between resonant frequency, minimum image jitter, and low variation in strut loading over the operating range. Optimum angle and height were determined to be 10º and 0.75 m respectively. This leads to an upper attachment diameter of 3.26 m at three equally spaced points. With this optimal geometry the strut loads vary from 15 kN at zenith to 40 kN tension and 27 kN compression at horizon pointing.

To accommodate the relatively large travel requirements for this hexapod we expect to use universal (Cardan) type end joints. The upper end joints are universal joints (2 DOF) while the lower joints include a rotational degree of freedom to allow the hexapod to position the payload without over-constraint. After comparing several commercially available actuators, we selected a commercial off-the-shelf actuator using a recirculating roller screw. This will be coupled to a harmonic drive gear reducer, servo motor, brake and encoder. This combination gave the best compromise between stiffness, backlash, low power consumption, and smooth operation at relatively low speeds. Brakes will be incorporated on each strut drive to prevent back driving. Two feedback devices are envisioned; rotary encoders on the drive motor shafts for feedback to the drive, and absolute linear encoders to measure the strut length directly.

The hexapod struts will be supplemented with frame members to hold the strut ends together allowing handling of the hexapod as an integral unit during installation. The frame members are structurally redundant and could be removed after installation. Pins matching radial slot features in the three upper strut mounting blocks will locate the hexapod to the telescope structure, while a similar arrangement will allow accurate repetition on installation of the M2 cell assembly.

Table 3. M2 positioner design requirements

Mass	<500 kg (goal)
Payload	>6,000 kg
Decenter, X, Range	+/- 15 mm
Decenter, Y, Range	+/- 15 mm
Decenter, specified as cylindrical radius, R	16 mm radius
Defocus, Z Range	+/- 17.5 mm
Tilt, rX,rY Range	+/- 2 mrad
Platform Z axis repeatability (precision)	1.24 m rms
Platform X,Y axis repeatability (precision)	0.43 m rms
Angular (rX,rY) repeatability (precision)	43 mas rms
System translation smoothness	0.43 m rms X,Y,Z
Angular rotation smoothness	43 mas rms tilt (rX,rY)
First Resonant Frequency (with payload)	15 Hz minimum
Slewing rate	33 m/sec (2mm/min)
Tilt Response Time slow tracking	0.53 arcsec per second time
Translation Response Time	100 micron per second time
Settle Time	250 ms

8. M3 POSITIONER

M3 will be actively controlled in tilt and rotation for pointing, slewing and tracking for each of the different Nasmyth platform instrument positions. The positioner will be able to point the beam to any given instrument on the Nasmyth platform within a time interval of 120 seconds maximum. Elapsed time is expected to be shorter for adjacent instrument positions. The Nasmyth platform instruments are located on both sides of the telescope at -6º to +28º from the Telescope elevation axis. M3 tilt and rotation trajectories for various Nasmyth instrument positions are shown in Figure 13.

The positioner will not extend outside of the shadow cast by the secondary. Several positioner configurations were considered leading to selection of the rotator/trunnion arrangement shown in Figure 14. The M3 positioner is inherently imbalanced about the tilt axis and can only be approximately balanced about the rotation axis. Over the range of tilt motion the payload center of mass varies ~20 mm either side of the rotation axis. A 950 kg counter-mass is included to balance the rotator payload at the median tilt position, bringing the entire rotator payload to 5500 kg. The countermass reduces the power required for rotation slews. The peak electrical power demand for the M3 positioner is expected to be 2.5 kW.

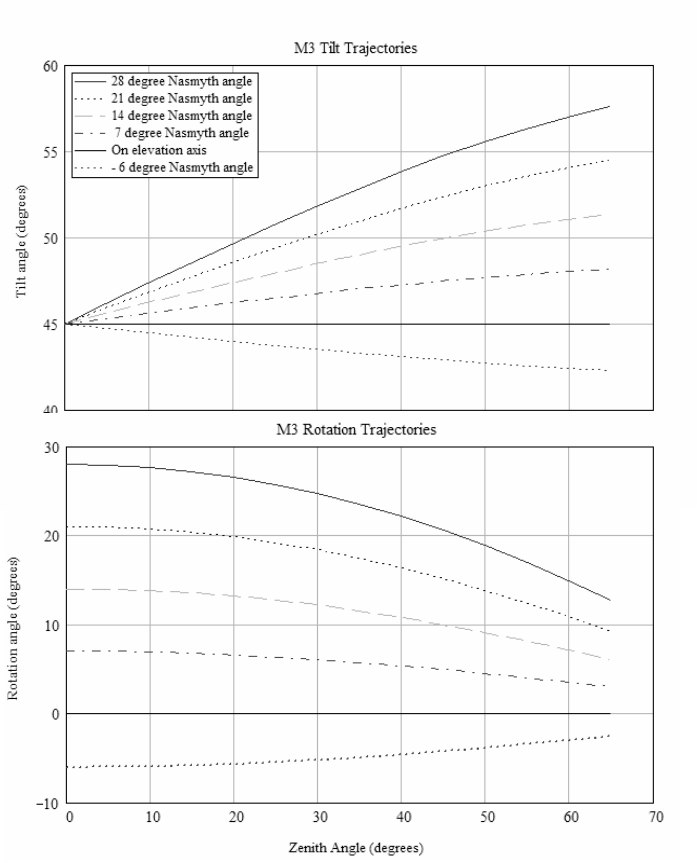

Figure 13. Tilt and rotation trajectories vary according to the position of the instrument on the Nasmyth platform.

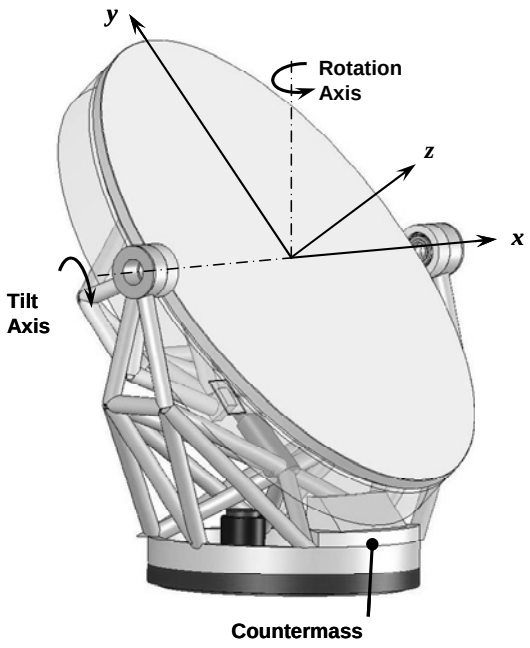

Figure 14. The M3 positioner will track in rotation and tilt to steer the beam to instruments on the Nasmyth platforms. Gravity loading on M3 follows a 3-space trajectory similar to an equatorially mounted optic. A countermass reduces the power required for slews.

The 2.0 m diameter rotator allows personnel and cable passage. Stiffness and smoothness are important design criteria for this bearing, though accuracy is not; run-out errors will be calibrated in the telescope pointing model and corrected via LUT's. An internal ring gear on the inner race of the bearing will mesh with two opposed rotator drives to reduce backlash. The drives rotate with the M3 structure while the internal ring gear and inner race of the bearing remain

stationary. A harmonic or planetary gear reducer will provide ~2600:1 reduction between the axis and the motor for smooth tracking at low tracking velocities. A tape encoder will be implemented on the inner diameter of the rotator bearing for position feedback. Power off brakes on the motor shafts will be included for safety and to further prevent back driving when the axis is not powered.

The tilt axis bearing set define a rotation axis that is nominally in the plane of the M3 surface. Here again stiffness and smoothness are important design criteria. Tilt actuation will use a commercial off-the-shelf roller or ball screw type linear actuator. The end pivot locations for this actuator will be located at structural nodes located on the rotator and tilt structures. A tape encoder will be implemented on a rail located on the tilt structure and will provide position feedback through an encoder head mounted on the rotator structure.

9. CONTROLS SYSTEMS

Control of the M2 and M3 systems has been developed in accordance with an *essential model*. In such a model, the designers assume that perfect technology is available and concentrate on the requirements of the system and how they are to be envisaged as a cohesive whole. It is a top-down approach—integrating hardware and software—that resolves sub-levels into finer detail. There is nothing in the model that implies a control hierarchy. A similar analysis applies to M3CS since both M2 and M3 require autonomous position control and figure control systems. The main difference between M2CS and M3CS is that M2CS will utilize a hexapod whereas M3CS will have an altitude over azimuth positioner.

Once the model is complete, one should consider a specific instance of the model using real hardware or software specifications as appropriate. In hardware terms, we have identified a choice of generic devices (CPU's, FPGA's or ASIC's) that can control multiple temperature sensors and thermal interlocks as well as figure control actuators and pressure sensors. For M2, six commercial off-the-shelf encoders will give absolute position with respect to the mirror cell. Pressure sensors and actuators for M2 are the subject of a vendor-supplied study and are proprietary. Eighteen load cells must be of sufficient capacity to accommodate combined axial and lateral loads. These will require 16-bit ADCs whereas the other 42 can be hosted by a local controller. The degrees of freedom for M2 and M3 are summarized in Table 4.

For the software we have identified data exchanges where data flows into and out of the model. There is no dynamic relationship implied (or, indeed, prohibited). So, for example, the telescope's alignment and phasing system (APS) will provide the data that converts into look-up tables but the actual conversion process is offline and not in real time. Conversely, the data exchange with the GMS occurs at the start of the observing night and in between observations.

Note that the software will be built upon the TMT common software to easily integrate into the observatory wide system. In routine operation, the M2CS and M3CS are considered sub-systems of the telescope supervisory controller (TSC) and will be fed by 20 Hz demand positions in the local coordinate system. Further correction due to specific controls systematic effects will be handled locally.

Table 4. Degrees of freedom for local control on-board the mirror cells. Both M2 and M3 will have similar provisions.

Controls Type	Component	DOF
Input	Encoders	6
Input	60 x 6 axis Load Cells	360
Input	Pressure Sensors	24
Output	Axial Support	24
Output	Lateral/Cross Supports	3

10. M2 AND M3 PRODUCTION SCHEDULE

Several mirror blank suppliers have provided production schedules that propose a 24-month delivery schedule from the release of the production contract. No attempt has yet been made to determine the capability of a single vendor to produce both optics during this two-year production period.

Polishing of M2 and M3 must be completed within two years after receipt of the mirror blanks if we are to allow time for a support system integration test at the polishing vendor prior to shipping the mirror blanks to site. Several polishing houses have supplied initial rough estimates that meet the two-year schedule.

The project schedule shows delivery of the M2 and M3 systems to site in time to support the alignment of the primary mirror segments. Up to a year of schedule slack could be developed if a prime focus camera is used for the initial M1 segment alignment. Integration of the M2 and M3 production schedule with the M1 installation schedule will be key to understanding the M2 and M3 production schedule constraints.

ACKNOWLEDGMENTS

The authors gratefully acknowledge the support of the TMT partner institutions. They are the Association of Canadian Universities for Research in Astronomy (ACURA), the Association of Universities for Research in Astronomy (AURA), the California Institute of Technology and the University of California. This work was supported, as well, by the Canada Foundation for Innovation, the Gordon and Betty Moore Foundation, the National Optical Astronomy Observatory, which is operated by AURA under cooperative agreement with the National Science Foundation, the Ontario Ministry of Research and Innovation, and the National Research Council of Canada.

REFERENCES

1. B. L. Ellerbroek, C. Boyer, C. Bradley, M. C. Britton, S. Browne, R. A. Buchroeder, J.-L. Carel, M. K. Cho, M. R. Chun, R. Claire, R. Conan, L. G. Daggert, R. G. Dekany, J. H. Elias, D. A. Erickson, R. Flicker, D. T. Gavel, L. Gilles, P. Hampton, G. Herriot, M. R. Hunten, R. R. Joyce, M. Liang, B. A. Macintosh, R. Palomo, I. P. Powell, S. C. Roberts, E. Ruch, J. Sinquin, M. J. Smith, J. A. Stoesz, M. Troy, G. A. Tyler, J.-P. Veran, C. R. Vogel, and Q. Yang, "A conceptual design for the Thirty Meter Telescope adaptive optics system", *Advances in Adaptive Optics II*, ed. Brent L. Ellerbroek and Domenico Bonaccini Calia, vol. 6272, SPIE, Orlando, 2006.

2. K. Vogiatzis, J. T. Fitzsimmons, M. Sun, "Strategies for estimating mirror and dome seeing for TMT", *Modeling, Systems Engineering, and Project Management for Astronomy II*, ed. Martin J. Cullum and George Z. Angeli, vol. 6271, SPIE, Orlando, 2006.